Long Term Dynamics of Debris Objects in MEO

Marielle Pellegrino [(1)(2)], Daniel Scheeres[(1)], Brett Streetman [(2)]

[(1)] The University of Colorado Boulder, 431 UCB Boulder CO 80302 USA
[(2)] The Charles Stark Draper Laboratory, Inc., 555 Technology Square Cambridge MA 02139 USA

ABSTRACT

Medium Earth orbit is subject to destabilizing luni-solar resonances due to the gravity of the Moon and Sun. This paper analyses this region using several different methods to calculate the drift between initial conditions. We also examine the how high area to mass ratio (HAMR) objects behave in this region and the interaction between solar radiation pressure and resonant dynamics. This enables us to have a better understanding of the long term dynamics of this region.

1 INTRODUCTION

From bank transactions to missile launches, our current world relies heavily on the use of global navigation satellite systems (GNSS). However, satellites in this orbital regime are subject to destabilizing resonances from the Sun and Moon which cause chaotic behavior in the long-term evolution of orbits in this region [1][2]. This long-term behavior poses a risk to maintaining the orbital environment for years to come. Retired satellites and debris can collide with functioning satellites in future decades if we do not take the steps now in understanding the long-term dynamics of orbital debris in medium Earth orbit (MEO). This paper will seek to study the evolution of orbits in MEO in both the satellites that are currently in it, namely heavy GNSS satellites, and the potential orbital debris that may inhabit the region, including high area to mass ratio (HAMR) objects.

To characterize the evolution of orbital debris, we will utilize numerical solutions that use doubly averaged dynamics. To appropriately study debris objects at high altitudes, the effect of solar radiation pressure (SRP) on these objects will also be considered, including HAMR objects. SRP is known to be a dominant effect on HAMR objects in geostationary orbit contributing to much of the debris in that region [3]. This work will preemptively consider the effects due to SRP in the dynamics of HAMR objects that may inhabit MEO. As HAMR objects are thought to often be mylar sheets separated from older satellites, and may be present in this region as existing satellites age.

There has been recent work in understanding the coupled effects of tesseral resonances and solar radiation pressure of the LEO region [4]. Other work has been done on understanding the combined effect of lunisolar and tesseral resonances and SRP but specfically in the geosynchronous orbit [5]. This paper will seek to understand the effects combining luni-solar resonances and solar radiaion pressure in medium Earth orbital regime.

2 DYNAMICS MODEL

The dynamics of this system are modeled using two forms of averaging. The effects due to the oblateness of the Earth is singly averaged, or averaged about the satellites mean anomaly. The effects due to solar radiation pressure and third bodies are doubly averaged or averaged about the perturbing bodies mean anomaly in addition to averaging about the satellite's mean anomaly [6].

These averaged solutions are described in terms of the Milankovitch elements, Equations 1 and 2.

$$\boldsymbol{e} = \frac{1}{\mu}\boldsymbol{v} \times \boldsymbol{H} - \hat{\boldsymbol{r}} \tag{1}$$

$$\boldsymbol{h} = \frac{\boldsymbol{r} \times \boldsymbol{v}}{\sqrt{\mu a}} \tag{2}$$

where $\boldsymbol{e}$ is the eccentricity vector and $\boldsymbol{h}$ is the scaled angular momentum vector. The velocity vector is denoted by $\boldsymbol{v}$, angular momentum by $\boldsymbol{H}$, position vector by $\boldsymbol{r}$, and semimajor axis by a. Together these vectors define eccentricity, inclination, argument of periapsis, and longitude of the ascending node.

2.1 J2

The perturbing acceleration due to the oblateness of the Earth is characterized by

$$\dot{\boldsymbol{h}}_{20} = -\frac{3nC_{20}}{2a^2h^5}(\hat{\boldsymbol{p}}\cdot\boldsymbol{h})\tilde{\hat{\boldsymbol{p}}}\cdot\boldsymbol{h} \tag{3}$$

$$\dot{\boldsymbol{e}}_{20} = -\frac{3nC_{20}}{4a^2h^5}\left(\left(1-\frac{5}{h^2}(\hat{\boldsymbol{p}}\cdot\boldsymbol{h})^2\right)\tilde{\boldsymbol{h}} + 2(\hat{\boldsymbol{p}}\cdot\boldsymbol{h})\tilde{\hat{\boldsymbol{p}}}\right)\cdot\boldsymbol{e} \tag{4}$$

where C_{20} is the second degree zonal gravitational coefficient, -.0010826269. The z axis of the Earth is represented by $\hat{\boldsymbol{p}}$ and μ is the gravitational parameter of the Earth, 398600 $\frac{\mathrm{km}^3}{\mathrm{s}^2}$.

2.2 Solar Radiation Pressure

The perturbing acceleration due to solar radiation pressure is defined by

$$\dot{\boldsymbol{h}}_{srp} = -\frac{2\pi(1-\cos\Lambda)}{T_s\cos\Lambda}\tilde{\hat{\boldsymbol{H}}}_{\boldsymbol{s}}\cdot\boldsymbol{h} \tag{5}$$

$$\dot{\boldsymbol{e}}_{srp} = -\frac{2\pi(1-\cos\Lambda)}{T_s\cos\Lambda}\tilde{\hat{\boldsymbol{H}}}_{\boldsymbol{s}}\cdot\boldsymbol{e} \tag{6}$$

where the SRP parameter is defined as

$$\tan\Lambda = \frac{3(1+\rho)P_0}{2V_{lc}H_sB} \tag{7}$$

where V_{lc} is the local circular speed of the orbiter, H_s is the norm of the Sun's angular momentum, and T_s is the Earth's orbital period about the Sun. This effect of the Sun's light is characterized by the pressure term, $P_0 = 1*10^8\frac{\mathrm{kg}*\mathrm{km}^3}{\mathrm{s}^2*\mathrm{m}^2}$.The ratio of reflectively, ρ, describes one of the material properties of the surface of the satellite, specifically how the Sun's light is reflected and in our model is set to 1. The mass-to-area ratio, B, also affects how strongly the satellite is influenced by SRP and is computed as $B = \frac{mass}{area}\frac{\mathrm{g}}{\mathrm{m}^2}$. Throughout the paper, we will reference the area-to-mass ratio which is the inverse of this parameter.

2.3 Third Body Perturbation

The acceleration due to the gravitational forces of a perturbing body are exhibited by

$$\dot{\tilde{\boldsymbol{h}}} = -\frac{3\mu_p}{4na_p^3h_p^3}\hat{\boldsymbol{H}}_p\cdot(5\boldsymbol{ee}-\boldsymbol{hh})\cdot\tilde{\hat{\boldsymbol{H}}}_p \tag{8}$$

$$\dot{\tilde{\boldsymbol{e}}} = -\frac{3\mu_p}{4na_p^3h_p^3}\left(\hat{\boldsymbol{H}}_p\cdot(5\boldsymbol{eh}-\boldsymbol{he})\cdot\tilde{\hat{\boldsymbol{H}}}_p - 2\tilde{\boldsymbol{h}}\cdot\boldsymbol{e}\right) \tag{9}$$

where a_p is the semimajor axis of the perturbing body, h_p is the scaled angular momentum of the perturbing body and $\hat{\boldsymbol{H}}_p$ is the unit vector of the angular momentum of the perturbing body.

3 DEVIATION DESCRIPTION

Before we delve into the different methods for analyzing chaos, we will discuss what is at the core of each of these methods, how the deviation is described. For each method, the deviation was calculated by integrating the models linearized equations, Equation 10.

$$\Delta\dot{x} = A\Delta x \tag{10}$$

where

$$A = \begin{bmatrix} \frac{\partial\dot{\boldsymbol{e}}}{\partial\boldsymbol{e}} & \frac{\partial\dot{\boldsymbol{e}}}{\partial\boldsymbol{h}} \\ \frac{\partial\dot{\boldsymbol{h}}}{\partial\boldsymbol{e}} & \frac{\partial\dot{\boldsymbol{h}}}{\partial\boldsymbol{h}} \end{bmatrix} \tag{11}$$

3.1 Initial Deviations

When perturbing the initial conditions, it is important that we maintain the properties of the Milankovitch elements. Those two properties being for initial conditions $\boldsymbol{e}_0$ and $\boldsymbol{h}_0$:

$$\boldsymbol{e}_0 \cdot \boldsymbol{h}_0 = 0 \tag{12}$$

$$\boldsymbol{e}_0 \cdot \boldsymbol{e}_0 + \boldsymbol{h}_0 \cdot \boldsymbol{h}_0 = 1 \tag{13}$$

And thus

$$(\boldsymbol{e}_0 + \Delta\boldsymbol{e}) \cdot (\boldsymbol{h}_0 + \Delta\boldsymbol{h}) = 0 \tag{14}$$

$$(\boldsymbol{e}_0 + \Delta\boldsymbol{e}) \cdot (\boldsymbol{e}_0 + \Delta\boldsymbol{e}) + (\boldsymbol{h}_0 + \Delta\boldsymbol{h}) \cdot (\boldsymbol{h}_0 + \Delta\boldsymbol{h}) = 1 \tag{15}$$

Therefore

$$\boldsymbol{h}_0 \cdot \Delta\boldsymbol{e} + \boldsymbol{e}_0 \cdot \Delta\boldsymbol{h} = 0 \tag{16}$$

$$\boldsymbol{e}_0 \cdot \Delta\boldsymbol{e} + \boldsymbol{h}_0 \cdot \Delta\boldsymbol{h} = 0 \tag{17}$$

and so the initial deviations, $\Delta\boldsymbol{e}$ and $\Delta\boldsymbol{h}$, must be perpendicular to the initial conditions, $\boldsymbol{e}_0$ and $\boldsymbol{h}_0$.

4 A MATRIX

To propagate the deviation forward in time we use the linearized dynamics which are derived by the following equations.

4.1 SRP

$$\frac{\partial \dot{\boldsymbol{e}}_{\boldsymbol{srp}}}{\partial \boldsymbol{e}} = -\frac{2\pi(1-\cos\Lambda)}{T_s \cos\Lambda} \tilde{\hat{\boldsymbol{H}}}_{\boldsymbol{s}} \tag{18}$$

$$\frac{\partial \dot{\boldsymbol{h}}_{\boldsymbol{srp}}}{\partial \boldsymbol{h}} = -\frac{2\pi(1-\cos\Lambda)}{T_s \cos\Lambda} \tilde{\hat{\boldsymbol{H}}}_{\boldsymbol{s}} \tag{19}$$

where the SRP parameter is defined as

$$\tan\Lambda = \frac{3(1+\rho)P_0}{2V_{lc}H_s B} \tag{20}$$

4.2 J2

$$\frac{\partial \dot{\boldsymbol{e}}_{\boldsymbol{20}}}{\partial \boldsymbol{e}} = -\frac{3nC_{20}}{4a^2h^5}\left[\left(1 - \frac{5}{h^2}(\hat{\boldsymbol{p}} \cdot \boldsymbol{h})^2\right)\tilde{\boldsymbol{h}} + 2(\hat{\boldsymbol{p}} \cdot \boldsymbol{h})\tilde{\hat{\boldsymbol{p}}}\right] \tag{21}$$

where $\hat{p}$ is the Earth's rotational axis.

$$\begin{aligned}\frac{\partial \dot{\boldsymbol{e}}_{\boldsymbol{20}}}{\partial \boldsymbol{h}} = -\frac{15nC_{20}\boldsymbol{h}}{4a^2h^7}&\left[\left(1 - \frac{5}{h^2}(\hat{\boldsymbol{p}} \cdot \boldsymbol{h})^2\right)\tilde{\boldsymbol{h}} + 2(\hat{\boldsymbol{p}} \cdot \boldsymbol{h})\tilde{\hat{\boldsymbol{p}}}\right] \cdot \boldsymbol{e} - \\ &\frac{3nC_{20}}{4a^2h^5}\left[\frac{10\boldsymbol{h}}{h^4}(\hat{\boldsymbol{p}} \cdot \boldsymbol{h})^2\tilde{\boldsymbol{h}} \cdot \boldsymbol{e} - \frac{10}{h^2}(\hat{\boldsymbol{p}} \cdot \boldsymbol{h})\hat{\boldsymbol{p}}\tilde{\boldsymbol{h}} \cdot \boldsymbol{e} - \right. \\ &\left.\left(1 - \frac{5}{h^2}(\hat{\boldsymbol{p}} \cdot \boldsymbol{h})^2\right)\tilde{\boldsymbol{e}} + 2(\tilde{\hat{\boldsymbol{p}}} \cdot \boldsymbol{e})\hat{\boldsymbol{p}}\right]\end{aligned} \tag{22}$$

$$\frac{\partial \dot{\boldsymbol{h}}_{\boldsymbol{20}}}{\partial \boldsymbol{h}} = \frac{15nC_{20}\boldsymbol{h}}{2a^2h^7}(\hat{\boldsymbol{p}} \cdot \boldsymbol{h})\tilde{\hat{\boldsymbol{p}}} \cdot \boldsymbol{h} - \frac{3nC_{20}}{2a^2h^5}(\hat{\boldsymbol{p}} \cdot \boldsymbol{h})\tilde{\hat{\boldsymbol{p}}} - \frac{3nC_{20}}{2a^2h^5}(\tilde{\hat{\boldsymbol{p}}} \cdot \boldsymbol{h})\hat{\boldsymbol{p}} \tag{23}$$

4.3 3rd Body

$$\frac{\partial \dot{\boldsymbol{e}}_{\boldsymbol{p}}}{\partial \boldsymbol{e}} = -\frac{3\mu_p}{4na_p^3h_p^3}\big[5(\boldsymbol{h}\cdot\tilde{\hat{\boldsymbol{H}}}_{\boldsymbol{p}})\hat{\boldsymbol{H}}_{\boldsymbol{p}} + (\hat{\boldsymbol{H}}_{\boldsymbol{p}}\cdot\boldsymbol{h})\tilde{\hat{\boldsymbol{H}}}_{\boldsymbol{p}} - 2\tilde{\boldsymbol{h}}\big] \tag{24}$$

where h_p is the scaled angular momentum of the perturbing body and H_p is the angular momentum of the perturbing body.

$$\frac{\partial \dot{\boldsymbol{e}}_{\boldsymbol{p}}}{\partial \boldsymbol{h}} = \frac{3\mu_p}{4na_p^3h_p^3}\big[5(\hat{\boldsymbol{H}}_{\boldsymbol{p}}\cdot\boldsymbol{e})\tilde{\hat{\boldsymbol{H}}}_{\boldsymbol{p}} + (\boldsymbol{e}\cdot\tilde{\hat{\boldsymbol{H}}}_{\boldsymbol{p}}\hat{\boldsymbol{H}}_{\boldsymbol{p}} - 2\tilde{\boldsymbol{e}}\big] \tag{25}$$

$$\frac{\partial \dot{\boldsymbol{h}}_{\boldsymbol{p}}}{\partial \boldsymbol{e}} = -\frac{3\mu_p}{4na_p^3h_p^3}\big[-(\hat{\boldsymbol{H}}_{\boldsymbol{p}}\cdot\boldsymbol{e})\tilde{\hat{\boldsymbol{H}}}_{\boldsymbol{p}} + (\boldsymbol{e}\cdot\tilde{\hat{\boldsymbol{H}}}_{\boldsymbol{p}})\hat{\boldsymbol{H}}_{\boldsymbol{p}}\big] \tag{26}$$

$$\frac{\partial \dot{\boldsymbol{h}}_{\boldsymbol{p}}}{\partial \boldsymbol{e}} = \frac{3\mu_p}{4na_p^3h_p^3}\big[(\hat{\boldsymbol{H}}_{\boldsymbol{p}}\cdot\boldsymbol{h})\tilde{\hat{\boldsymbol{H}}}_{\boldsymbol{p}} + (\boldsymbol{h}\cdot\tilde{\hat{\boldsymbol{H}}}_{\boldsymbol{p}})\hat{\boldsymbol{H}}_{\boldsymbol{p}}\big] \tag{27}$$

5 METHODS FOR CALCULATING CHAOS

We will utilize three different methods to evaluate chaos at GPS orbits. One utilizes Lyapunov time which is defined as the inverse of the largest Lyapunov exponent. The other two are different ways to evaluate the largest Lyapunov exponent.

5.1 Lyapunov Time

The first method evaluates the system in terms of Lyapunov time which is defined as the inverse of the Lyapunov exponent. To calculate Lyapunov time we take the magnitude of the deviation at each time step of the arc. We then take the logarithm of this set of numbers. Finally, we take the supremum of the arc to find the Lyapunov time for the simulation. This method is to match the same computation method Daquin uses to define chaos [7].

$$FLI(t) = \sup_{\tau\leq t} \ln\big\|\Delta x(\tau)\big\| \tag{28}$$

For these maps, the starting time is the J200 date. They initialize with a Galileo semimajor axis, a RAAN of 120 degrees, and an argument of perigee of 30 degrees. There are a set of 300 eccentricities ranging from .01 to .5 versus 300 initial inclinations between 50 and 75 degrees. The simulation finishes after 200 years

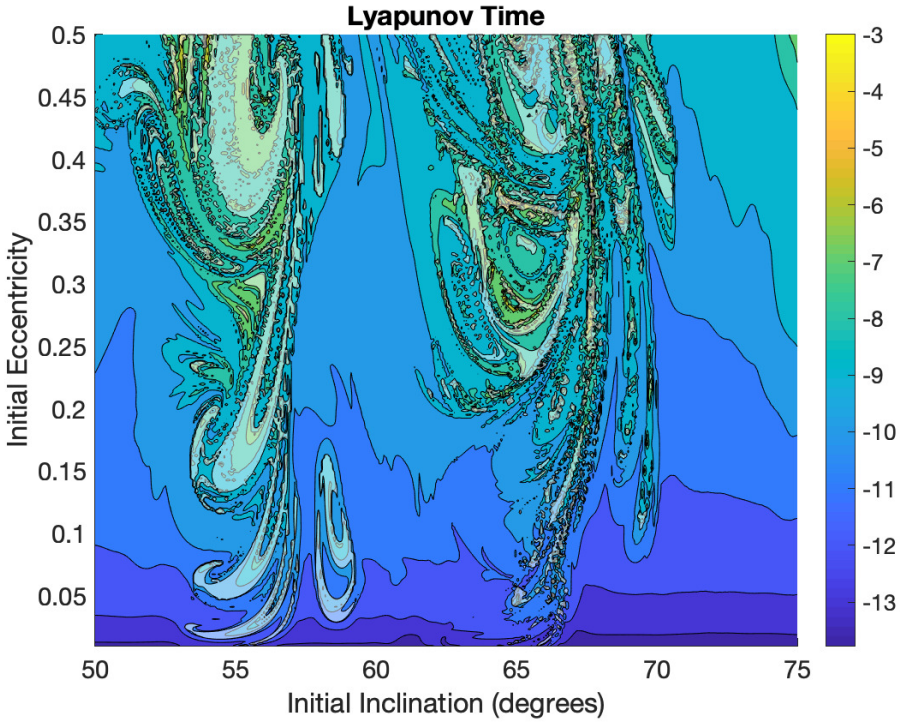

Fig. 1. Contour map of Lyapunov times. Shaded regions indicate Earth reentry before end of simulation.

5.2 Generic Lyapunov Exponent

The following Lyapunov solver is the simplest method for measuring the change in deviation. This method involves normalizing the magnitude of the deviation by the initial magnitude of the deviation. Then taking the logarithm of that value over each time arc. Finally we divide by the length of time over the entire arc and take the supremum of this set. Larger Lyapunov exponents indicate regions of chaos and smaller ones indicate regions of stability.

$$\mu = \sup \frac{1}{t} \ln \frac{\|\Delta x(t)\|}{\|\Delta x_0\|} \tag{29}$$

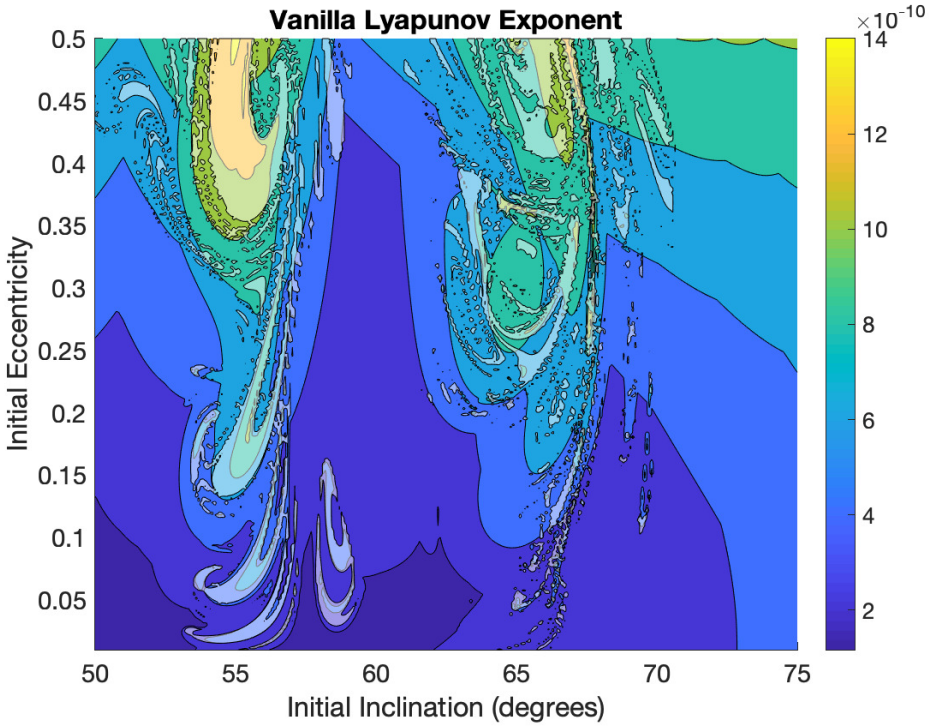

Fig. 2. Contour map of Lyapunov exponents calculated using the generic algorithm. Shaded regions indicate Earth reentry before end of simulation.

5.3 Benettin Lyapunov Exponent

Instead of letting the solution deviate from the initial point over the entire arc, the Benettin method for solving Lyapunov exponents normalizes the deviation after each time. This means that while the other methods find the supremum over the entire arc, the Benettin method has several smaller arcs these values are calculated over which are all summed together to solve for the Lyapunov exponent for the particular point. Figure **??** shows a schematic of the algorithm taken from Kuznetsov where the deviation is indicated by $\tilde{x}$ where we use Δx [8].

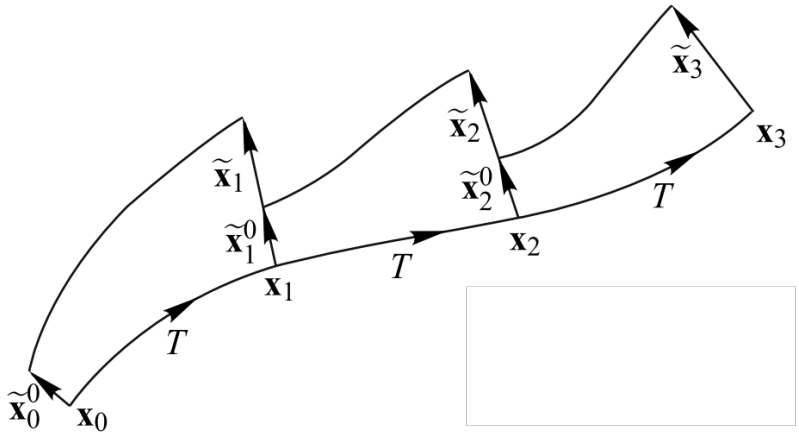

Fig. 3. Normalization of the deviation using the Benettin algorithm [8].

$$\mu = \frac{1}{MT}\sum_{i=1}^{M} \ln\|\Delta x_i\| \tag{30}$$

where M is the number of intervals the deviation is normalized for, in this case 20 intervals. T is the time span for each interval, 500 years/20.

We have slightly adjusted this equation to take the supremeum over the arc and normalize by that value.

$$\mu = \frac{1}{MT}\sum_{i=1}^{M} \sup \ln \frac{\|\Delta x_i\|}{\|\Delta x_{i0}\|} \tag{31}$$

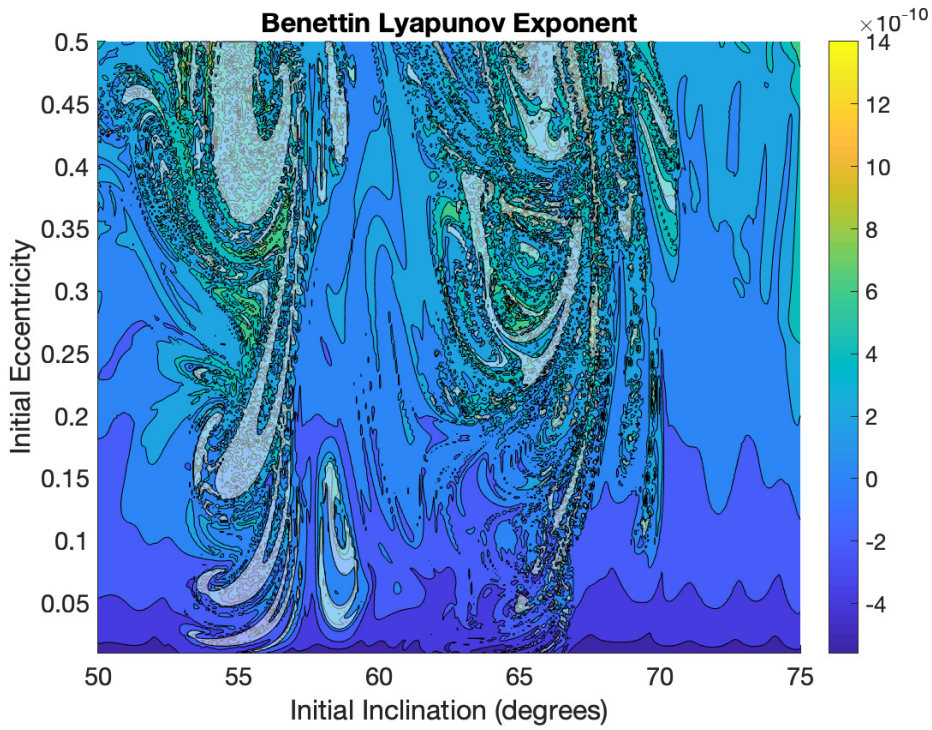

Fig. 4. Contour map of Lyapunov exponents calculated using the Benettin algorithm. Shaded regions indicate Earth reentry before end of simulation.

6 HAMR OBJECTS

The previous simulations have all been done with area to mass ratio are comparable to GPS satellites with a value of about .02 m^2/kg. However, if we utilize area to mass ratio's closer to what we see of debris. In particular, the outer layers of MLI are about 6 m^2/kg and the inner layers of MLI are about 110 m^2/kg [9].

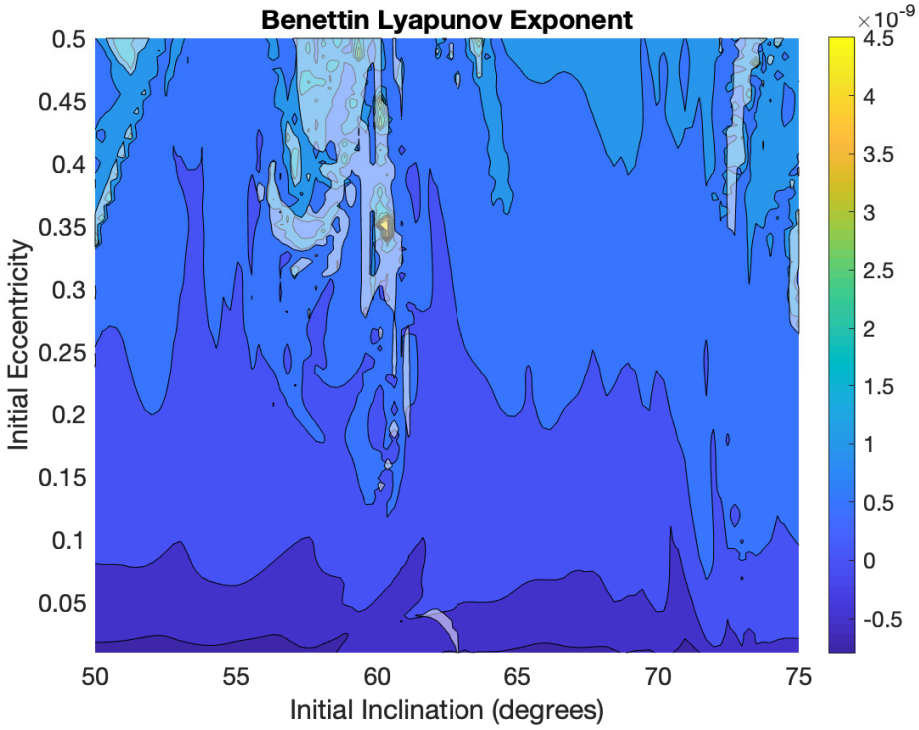

Fig. 5. Lyapunov exponent using the Benettin algorithm for a HAMR object with 6 m^2/kg area to mass ratio shaded regions indicate Earth reentry

For area to mass ratios higher than about 10 m^2/kg we found the assumptions used in the formulation of the doubly averaged SRP equations doe not hold. Therefore for the inner layers of MLI we use the singly averaged formulation for the SRP perturbation [5].

$$\dot{\boldsymbol{h}}_{srp} = -\frac{3}{2}\sqrt{\frac{a}{\mu}}\frac{P_0(1+\rho)}{Bd^2}\tilde{\hat{\boldsymbol{d}}}_{\boldsymbol{s}} \cdot \boldsymbol{e} \tag{32}$$

$$\dot{\boldsymbol{e}}_{srp} = -\frac{3}{2}\sqrt{\frac{a}{\mu}}\frac{P_0(1+\rho)}{Bd^2}\tilde{\hat{\boldsymbol{d}}}_{\boldsymbol{s}} \cdot \boldsymbol{h} \tag{33}$$

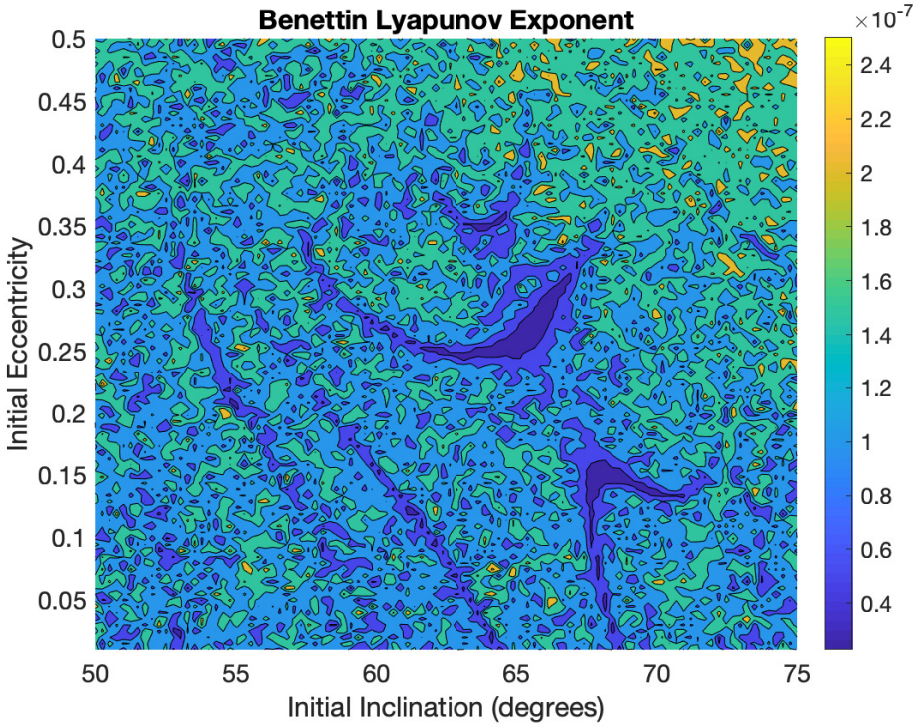

Fig. 6. Lyapunov exponent using the Benettin algorithm for a HAMR object with 100 m^2/kg area to mass ratio

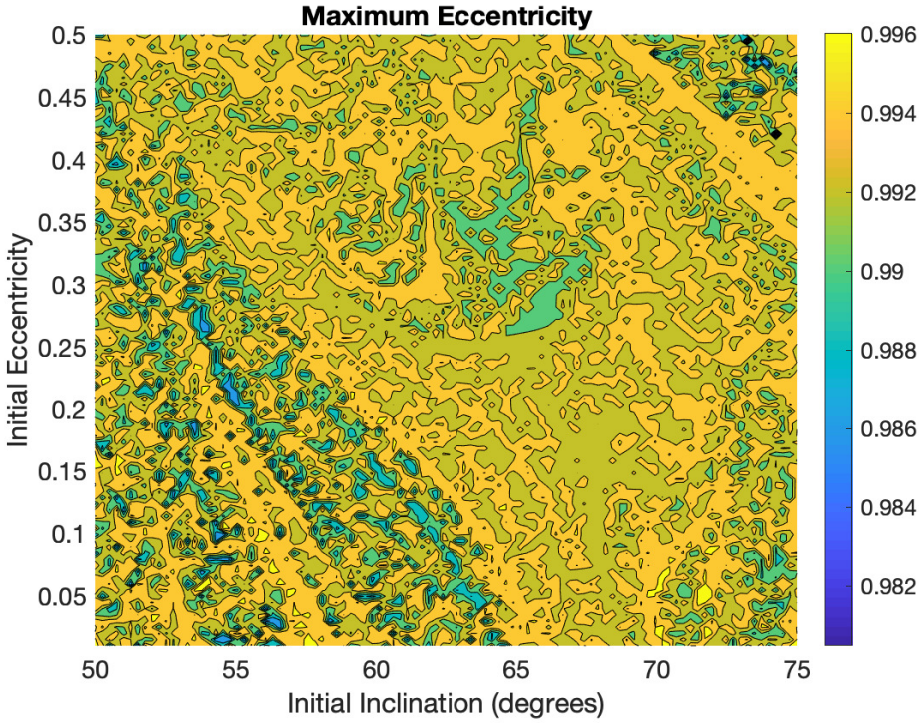

Fig. 7. Maximum Eccentricity for a HAMR object with 100 m^2/kg area to mass ratio

7 CONCLUSION

The three different methods for describing chaos show agreement. This helps validate the existence of chaos in this region and its sensitivity to initial conditions. All three methods confirm there is chaos with positive Lyapunov exponents and Lyapunov time, indicating nearby solutions diverge from each other rather than stabilizing on a final solution. The generic algorithm shows greater trends in the dynamics over the region, while the Benettin algorithm and Lyapunov time show greater detail between the regions.

Objects with high area to mass ratios show different behavior than the nominal GPS satellite's area to mass ratio. The increased effect due to solar radiation pressure shows guaranteed reentries for very high area to mass ratio object like the inner layers of MLI. For lower HAMR objects like the outer layers of MLI, there is an interaction and overall shift of the resonant dynamics and overall Earth reentries.

8 REFERENCES

1. Rosengren, A.J., Alessi, E.M., Rossi, A. and Valsecchi, G.B., "Chaos in navigation satellite orbits caused by the perturbed motion of the Moon", Monthly Notices of the Royal Astronomical Society, 449(4), pp.3522-3526 2015.

2. Alessi, E.M., Deleflie, F., Rosengren, A.J., Rossi, A., Valsecchi, G.B., Daquin, J., Merz, K,. "A numerical investigation on the eccentricity growth of GNSS disposal orbits", Celestial Mechanics and Dynamical Astronomy, 125(1), 71-90 2016.

3. Rosengren, A.J., Scheeres, D.J., McMahon, J.W., "The classical Laplace plane as a stable disposal orbit for geostationary satellites", Advances in Space Research, 53(8), pp 1219-1228, 2014.

4. Alessi, E.M., Colombo, C., Rossi, A., "Phase space description of the dynamics due to the coupled effect of the planetary oblateness and the solar radiation pressure perturbations." arXiv preprint 2019.

5. Casanova, D., Petit, A., Lemaître, A., "Long-term evolution of space debris under the J2 effect, the solar radiation pressure and the solar and lunar perturbations." Celestial Mechanics and Dynamical Astronomy, 123(2), 223-238, 2015.

6. Pellegrino, M.M., Scheeres D.J., and Streetman B.J., "Rapid Computation of MEO Satellite Deorbit Times Using Doubly Averaged Dynamics",International Astronautical Congress, Washington DC, USA, October 2019.

7. Daquin, J., et al. "The dynamical structure of the MEO region: long-term stability, chaos, and transport." Celestial Mechanics and Dynamical Astronomy 124.4, pp 335-366, 2016.

8. Kuznetsov S.P., *Hyperbolic Chaos: A Physicist's View*, Higher Education Press, Beijing and Springer- Verlag GmbH Berlin Heidelberg, 2012.

9. Früh, C., Kelecy, T.M., and Jah M.K., "Coupled orbit-attitude dynamics of high area-to-mass ratio (HAMR) objects: influence of solar radiation pressure, Earth's shadow and the visibility in light curves.", Celestial Mechanics and Dynamical Astronomy 117.4, 385-404, 2013.